Biochimica et Biophysica Acta 1807 (2011) 779–787

Contents lists available at ScienceDirect

Biochimica et Biophysica Acta

journal homepage: www.elsevier.com/locate/bbabio

Spectral components of the α-band of cytochrome oxidase

N. Kim, M.O. Ripple, R. Springett *

Department of Radiology, Dartmouth Medical School, Hanover, NH 03755, USA

ARTICLE INFO

Article history:
Received 18 October 2010
Received in revised form 11 March 2011
Accepted 15 March 2011
Available online 21 March 2011

Keywords:
Cytochrome oxidase
Redox titration
Midpoint potential
Optical spectroscopy
Proton pumping
Membrane potential

ABSTRACT

Oxidative redox titrations of the mitochondrial cytochromes were performed in near-anoxic RAW 264.7 cells by inhibiting complex I. Cytochrome oxidation changes were measured with multi-wavelength spectroscopy and the ambient redox potential was calculated from the oxidation state of endogenous cytochrome *c*. Two spectral components were separated in the α-band range of cytochrome oxidase and they were identified as the difference spectrum of heme *a* when it has a high (a_H) or low (a_L) midpoint potential (E_m) by comparing their occupancy during redox titrations carried out when the membrane potential ($\Delta\Psi$) was dissipated with a protonophore to that predicted by the neoclassical model of redox cooperativity. The difference spectrum of a_L has a maximum at 605 nm whereas the spectrum of a_H has a maximum at 602 nm. The $\Delta\Psi$-dependent shift in the E_m of a_H was too great to be accounted for by electron transfer from cytochrome *c* to heme *a* against $\Delta\Psi$ but was consistent with a model in which a_H is formed after proton uptake against $\Delta\Psi$ suggesting that the spectral changes are the result of protonation. A stochastic simulation was implemented to model oxidation states, proton uptake and E_m changes during redox titrations. The redox anti-cooperativity between heme *a* and heme a_3, and proton binding, could be simulated with a model where the pump proton interacted with heme *a* and the substrate proton interacted with heme a_3 with anti-cooperativity between proton binding sites, but not with a single proton binding site coupled to both hemes.

1. Introduction

Cytochrome oxidase (CytOx) is the terminal oxidase of the mitochondrial electron transport chain and is responsible for ≈90% of cellular oxygen consumption (recently reviewed in [1]). The X-ray structure has confirmed that electrons from cytochrome *c* (Cyt*c*) enter the enzyme at the Cu_A site which is located on the intermembrane side of the enzyme [2,3]. The electrons are transferred to the heme *a* center, which is located ≈1/3 into the inner membrane, and then parallel to the membrane to the binuclear center composed of heme a_3 and Cu_B where oxygen is reduced to water in a concerted 4-electron reduction. Part of the energy released on reduction of oxygen by Cyt*c* is conserved by pumping 4 protons per oxygen from the matrix to the intermembrane space against a proton motive force (ΔP). In many models, proton pumping is achieved by coupling the pK_a of a putative pumping site to the midpoint potential (E_m) of heme *a* and/or heme a_3 [4] although a model has been proposed in which the pK_a of the pump site is coupled to the pK_a of a second site via a conformational change in the protein [5]. A current focus of research is on elucidating the proton pathways and the mechanism of proton pumping [5–7]. However, a complete description of CytOx function must also include how CytOx dynamically varies its turnover rate depending on the energization of the inner membrane [8,9], how the apparent oxygen affinity for turnover is decreased in the functioning enzyme compared to the isolated enzyme[10] as well as how respiratory control is altered by the possible phosphorylation of CytOx under control of signaling pathways [11]. Such a description requires a detailed knowledge of the properties of the redox centers and their relationship to the membrane potential ($\Delta\Psi$) and pH gradient across the inner membrane.

The early classical model postulated that heme *a* and heme a_3 were independent redox centers and that their spectral contributions to the Soret band were approximately equal whereas heme *a* dominated in the α-band [12]. Later work performing redox titrations using the α-band region in the absence [13] and presence [14] of ΔP found two $n=1$ redox transitions each with a distinct spectral signature which were assigned to heme *a* and heme a_3. In order to account for spectral changes on ligand binding, the authors concluded that there were considerable spectral interactions between heme *a* and heme a_3 in the α-band region. Later work, which took into account the results of redox titrations using EPR spectroscopy and optical spectroscopy of the Soret- and α-band features, concluded that heme a_3 makes little contribution to the absorption spectrum in the α-band region and that the non-Nernst relationship observed in α-band redox titrations was the result of anti-cooperative redox interactions between the heme *a* and heme a_3 [15]. This culminated in the neoclassical model in which the spectral

Abbreviations: a_H, high potential or protonated heme *a*; a_L, low potential or unprotonated heme *a*; E_m, midpoint potential

* Corresponding author at: HB7786 Vail, Hanover, NH 03755, USA. Fax: +1 603 650 1717.
E-mail address: RSpringett@Dartmouth.edu (R. Springett).

0005-2728/$ – see front matter © 2011 Elsevier B.V. All rights reserved.
doi:10.1016/j.bbabio.2011.03.008

properties of heme *a* and heme a_3 are independent and heme *a* and heme a_3 have a high E_m when the other center is oxidized (typically 360 mV) and a low E_m when the other center is reduced (typically 240 mV) [16]. Redox titrations performed with Raman spectroscopy [17], magnetic circular dichroism [18] and infrared spectroscopy [19], where multiple redox centers can be followed, have shown and confirmed the redox anti-cooperativity between heme *a* and heme a_3 but the origin of the spectral changes in the α-band region of CytOx has not been determined. Attempts have been made to extend the neoclassical model to include Cu_B [20,21] and Cu_A [21,22].

Electrostatic calculations have suggested that the anti-cooperativity can be explained in terms of simple electrostatic repulsion between the hemes [23]. However, these calculations do not take into account the uptake of protons which would tend to shield the charge on the hemes. Alternatively, a recent kinetic study in which electron transfer and proton transfer were followed in real time has introduced the concept that the midpoint potentials of heme *a*, heme a_3 and Cu_B are dependent on protonation events [24]. Electrons were injected into the Cu_A center with nanosecond temporal precision and four phases of electron and proton movements were observed. The first phase ($\tau = 10$ μs) involves electron equilibration between Cu_A and heme *a* in which heme *a* and heme a_3 have midpoint potentials of 270 mV and <130 mV. The second phase ($\tau = 150$ μs) involves uptake of the pumped proton to a site estimated to be above the hemes which raises the E_m of heme *a* and heme a_3 to +360 mV and results in equilibration of the electron between the three centers. During the first two phases, Cu_B acts with a midpoint of <130 mV but the substrate proton uptake in the third phase ($\tau = 800$ μs) raises the E_m of Cu_B to >460 mV and results in complete transfer of the electron to Cu_B. The final phase ($\tau = 2400$ μs) involves release of the pumped proton into the p-side of the membrane.

Recently, we have developed an optical spectroscopy system that can measure oxidation changes of the cytochromes of the bc_1 complex, Cyt*c* and CytOx from the change in attenuation spectrum of living cells in suspension [25]. The advantage of performing these measurements in cells rather than isolated mitochondria is that the mitochondria in living cells are operating under genuine physiological conditions. Our overall goal is to develop and validate a kinetic model of CytOx that can account for changes in the apparent oxygen affinity for turnover, the dependence of turnover on $\Delta\Psi$, pH gradient and Cyt*c* redox potential and how this dependence can be altered under the control of cell signaling pathways. Such a model can only be validated in a system in which CytOx pumps against a physiological membrane potential. Furthermore, a cell model is essential to examine the effects of cytosolic signaling pathways on mitochondrial function. The goal of the studies presented here is to quantify and interpret the spectral changes that occur in the α-band range of CytOx and to reconcile the neoclassical model with proton–electron interactions revealed from the more recent kinetic studies.

In this work, carried out on RAW 264.7 mouse macrophage cells, it is shown that there are two distinct but overlapping spectral components in the α-band range of CytOx. These components are separated into the familiar 605 nm band of heme *a* which we label a_L and a previously unassigned 602 nm band which we label a_H. Within the framework of the neoclassical model, we show that the a_L and a_H components can be assigned to the difference spectrum of heme *a* when it has a low or high midpoint potential, respectively. Furthermore, we show that the shift in the E_m of a_H on de-energization of the inner membrane is too great to be accounted for by the movement of an electron from Cyt*c* to heme *a* against $\Delta\Psi$ but is consistent with a model in which a_H is formed after proton uptake against $\Delta\Psi$. Finally, we implement a stochastic simulation of CytOx reduction using the reaction constants determined from the kinetic study and show that it results in strong redox cooperativity between heme *a* and heme a_3 rather than anti-cooperativity and that it cannot account for the spectral changes observed during redox titrations if a_H is formed on binding of the pump proton. In contrast, a model in which (1) the pump proton interacts with heme *a* to raise its E_m forming a_H and (2) the substrate proton interacts with heme a_3 to raise its E_m reproduces both redox anti-cooperativity and the spectral changes if there is strong anti-cooperativity between the proton binding sites.

2. Experimental procedures

2.1. Cell culture and measurement chamber

RAW 264.7 mouse macrophage cells were cultured at 37 °C in 250 mL spinner flasks in phenol red-free RPMI medium with 10% fetal bovine serum and antibiotics/antimycotics in a 95% air / 5% CO_2 humidified incubator. Cells were spun down at 500 g for 5 min and resuspended at a concentration of 2.0×10^7 cells per mL in RPMI medium in a stirred 6 mL custom-built chamber that consisted of a quartz cylinder of inside diameter of 17 mm surrounded by water jacket to maintain the cells at 37 °C. The oxygen concentration was measured from the fluorescence lifetime of phosphorescent membrane (Tautheta Instruments, Boulder, CO) located at the bottom of the chamber.

The chamber was sealed with a stainless steel plunger and oxygen consumption measured from the depletion of oxygen (respirometry mode) or oxygenated and deoxygenated under computer control by passing a gas mixture of 5% CO_2 and a blend of N_2 and O_2 through 90 mm of fine-bore silicone tubing immersed in the cell suspension (oximetry mode). The tubing delivered oxygen to the suspension medium at a rate proportional to the difference in oxygen tension between inside the tubing and in the medium. Typically, the cells required an oxygen fraction of 0.40 in the tubing to match oxygen delivery to cellular consumption at an oxygen concentration of 100 μM.

2.2. Spectroscopy

The cells were illuminated with a white light emitting diode (NFSW036B, Nichia, Detroit, MI) and light was collected with 1 mm optical in remission geometry with a source-detector separation of 10 mm. The differential pathlength was measured using the 2nd differential technique from the 740 nm absorption band of water [26] and was found to be ≈39 mm. The output of the fiber was focused onto the slits of a Triax 320 spectrograph (HORIBA Jobin Yvon, Edison, NJ) and complete spectra were collected between 508 and 640 nm on a CCD (DV401BV, Andor Technology, South Windsor, CT). The pixel bandpass was ≈0.13 nm and the entrance slit width was set to give a spectral resolution of 1 nm.

2.3. Spectral analysis

The cytochrome oxidation changes were calculated by fitting a linear combination of model spectra to the change in attenuation spectrum. The model spectra were b_H, b_L and c_1, from the bc_1 complex, Cyt*c*, and a_L, a_H and a_3 from CytOx as well as a quadratic background to account for any baseline drift. Attenuation spectra are presented with the background subtracted but without smoothing. The difference spectra of heme a_3 and the familiar 605 nm form of heme a (a_L) were collected by Lao and Palmer [27] from the isolated bovine enzyme.

It was found that the anoxic-oxygenated difference spectra of the cells showed heme *a* predominately as a_H and could not be fitted as a combination of heme *a* and heme a_3 spectra [27] whereas CytOx became fully reduced after addition of FCCP under anoxic conditions (see Fig. 3). As heme *a* can be expected to be almost fully reduced under both anoxic conditions, the change in attenuation contains a component of the spectrum of $a_L + a_3 - a_H$ scaled by an arbitrary factor as well as small components due to oxidation changes in the other

cytochromes. The spectrum of $a_L + a_3 - a_H$ was extracted from the average change in attenuation spectrum of six independent experiments by first fitting a pair of Gaussians to the major feature at 609 nm between 590–630 nm. This spectrum, the other hemes and a quartic background spectrum was then fitted to the average attenuation spectrum and the spectrum of $a_L + a_3 - a_H$ was assumed to be the sum of Gaussians and the quartic background. The rationale for this procedure is that the hemes have sharp spectral features whereas the quartic background can account for the slowly varying features of $a_L + a_3 - a_H$ in the range 510–590 nm. Once the spectral shape of $a_L + a_3 - a_H$ was extracted from the attenuation spectrum, it was scaled by performing a non-linear least squares fit to the neoclassical model using the scaling factor as a fourth parameter and the spectrum of a_H calculated.

2.4. Stochastic simulations

A stochastic model based on Gillespie's algorithm [28] following Ransac et al. [29] but including interactions between states was implemented in Delphi 2010 using mixed object Pascal and assembly language. In brief, CytOx was modeled containing Cyt*c* binding site, four redox centers (Cu_A, heme *a*, heme a_3 and Cu_B) and either two or three protonation centers. The electrostatic or conformational interaction between reduced redox centers and protons were included by changing the forward and reverse rate constants when the interacting centers were both reduced and protonated. The models do not include electron–electron interactions between the redox centers as the goals were to show that proton–electron interactions can lead to the heme centers titrating as if electron–electron interactions were present. Great care was taken to ensure the energy of a state was independent of the reaction pathway by which that state was reached, that is, the models are thermodynamically consistent.

Two models were considered. Model I uses the parameters of a recent kinetic study in which the O to E reaction was followed in real time [24]. This model includes two proton binding sites, a pump site in which the proton interacts with heme *a* and heme a_3 and a substrate site in which the proton interacts with Cu_B. Model II uses the same parameters as model I except that the pump proton only interacts with heme *a* and a second substrate site is included which interacts with heme a_3. Electrostatic interactions are long ranged compared to the separation of the heme centers and only having the pump proton interact with heme *a* and the substrate protons interact with the binuclear center is an approximation but it allows the model to be as simple as possible. An additional reaction is included to allow the substrate proton to move rapidly between substrate sites. The energy levels and equilibration rates (defined as the sum of the forward and reverse rate) evaluated at a pH of 7.0, a Cyt*c* redox potential of 0 mV and setting the energy of the fully oxidized enzyme to 0 mV for the two models are summarized in Fig. 1. Fig. 1A shows docking of Cyt*c*, transfer of the electron to Cu_A and then heme *a* and uptake of the pump proton. These transitions are common to both models. Fig. 1B shows transfer of the electron from heme *a* to heme a_3, and then Cu_B with uptake of the substrate proton and release of the pump proton for model I. Fig. 1C shows the equivalent for model II consisting of electron transfer to heme a_3, uptake of the first substrate proton and release of the pump proton followed by transfer of the electron and substrate proton to Cu_B. The states in gray show energy levels without the proton–electron interactions. The interactions in both models are −210 mV for heme *a*, −350 mV for heme a_3 and −570 mV for Cu_B.

The temporal evolution of the enzyme on photo-induced reduction of Cu_A was simulated by initializing the model with the Cu_A center reduced, the Cyt*c* binding center empty, the other redox centers oxidized and the proton sites empty. The enzyme was allowed to evolve stochastically (excluding the Cyt*c* binding reactions) and the occupancy of each state was logged at 1 μs intervals for 10 ms of enzyme turnover. Charge transfer was calculated from the time-integral of electron transfer from Cu_A to heme *a* reaction and proton transfer reactions assuming the binuclear center and the pump site are located 34% and 25% from the cytosolic side of the membrane, respectively. An ensemble of enzymes was modeled by averaging the occupancy of each state at each time point over 10,000 separate simulations. Computational time was approximately 18 s on a six-core 3.2 GHz AMD Phenom II processor.

Redox titrations were simulated by allowing a single CytOx to interact with a thermodynamic pool of Cyt*c*. This was achieved by scaling the forward rate for reduced and oxidized Cyt*c* binding by the fraction that Cyt*c* would be reduced (f_r) or oxidized (f_o), respectively, at a given redox potential of the Cyt*c* pool. This is equivalent to varying the concentration of reduced and oxidized Cyt*c* appropriate to the redox potential of Cyt*c* assuming a first order forward reaction. The model was initialized with the Cyt*c* binding site empty, the redox centers oxidized and the proton binding sites empty. The enzyme was allowed to evolve stochastically for 10^8 partial reactions (a minimum of 80 s of enzyme turnover) and the time-weighted average occupancy of each state logged. Computational time was approximately 38 min for 55 redox potentials on a six-core 3.2 GHz AMD Phenom II processor. In both sets of simulations, a_H and a_L were defined as the states in which heme *a* was reduced and the pump site was protonated or unprotonated, respectively.

3. Results

3.1. Spectra

Cells were placed in the sealed chamber and allowed to consume the oxygen until they became anoxic whereupon 1 μM FCCP, a proton ionophore, was added to collapse ΔP. Fig. 2A shows the change in attenuation spectra between saturating oxygen concentration and anoxia before and after the addition of FCCP. Prior to addition of FCCP, the attenuation spectra showed a peak at 550 nm corresponding to the α-band of Cyt*c*, a shoulder at ≈560 nm corresponding to the α-band of the b-cytochromes from the bc_1 complex, a peak at ≈521 nm corresponding to the overlapping β-bands of Cyt*c*, c_1, b_H and b_L, and a peak at 602.4 nm in the α-band region of CytOx. The α-band of heme c_1 was not resolved from the more intense α-band of Cyt*c*. After FCCP, there were small changes at ≈536 nm and ≈560 nm and the α-band of CytOx increased in magnitude and shifted to 605 nm. The change in attenuation spectrum between saturating oxygen and anoxia prior to FCCP was poorly fitted by the spectra of heme a_L and heme a_3 as indicated by the residuals of the fit, whereas a good fit was found after addition of FCCP (see Fig. 2B).

The difference attenuation spectrum on addition of FCCP is shown in Fig. 2C. The difference spectrum is dominated by a band centered at ≈609 nm. The changes at 560 nm are resolved into a double peak which is characteristic of an oxidation of heme b_L. The component of the attenuation spectrum that the fitting algorithm attributes to heme b_L is overlaid. This component, along with much smaller components attributed to heme b_H, heme c_1 and Cyt*c*, was subsequently subtracted to give the difference spectrum of the fully reduced enzyme and a_H. The difference spectrum, which was calculated from the average of six difference spectra from independent experiments and scaled as described in the methods section, was subtracted from the spectrum of the fully reduced enzyme to give the spectrum of a_H. The spectrum of a_H is compared to the difference spectra of heme *a* (assumed to be a_L) and heme a_3, both measured from the bovine enzyme [27], in Fig. 2D. The spectra of a_H and a_L have peaks at 602.1 and 605 nm, respectively, and have the same 630 nm-peak intensity to within 3%.

Fig. 3 shows temporal traces of cytochrome oxidation changes when the heme a_H and a_L spectra were included in the decomposition algorithm. The cells consumed oxygen in the chamber until anoxia at 0 min and then 1 μM of FCCP was added at 2 min. At high oxygen

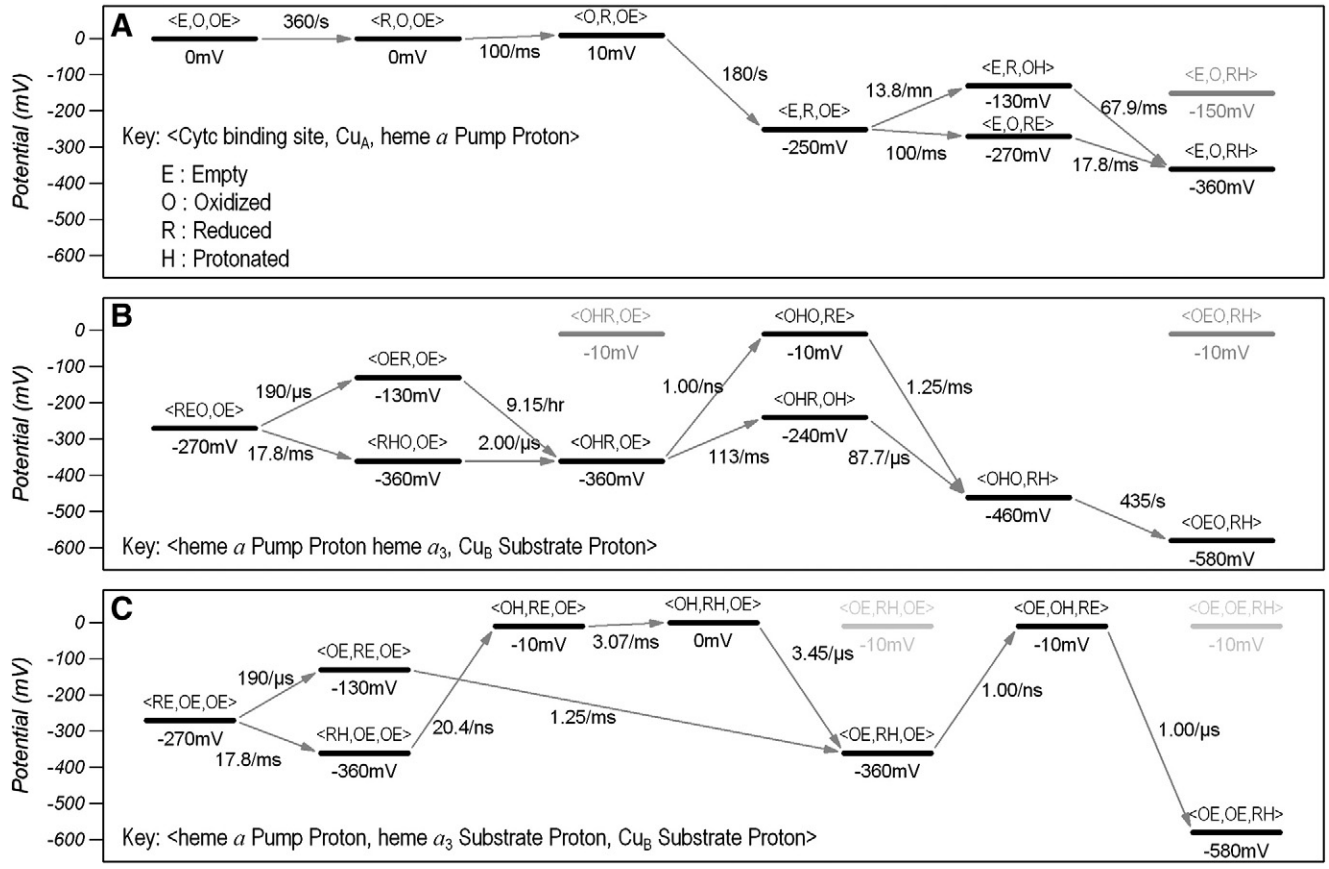

Fig. 1. The energy levels and equilibration rates (defined as the sum of the forward and reverse rate) evaluated at a pH of 7.0 and a Cyt*c* redox potential of 0 mV for the two stochastic models. The states are described in the key where the Cyt*c* binding site can either be empty (E), bound with reduced Cyt*c* (R) or bound with oxidized Cyt*c* (O); Cu_A, heme *a*, heme a_3 and Cu_B can either be oxidized (O) or reduced (R) and the proton sites can either be empty (E) or protonated (H). The energy of states without electron–proton interactions are shown in gray. (A) Docking of Cyt*c*, transfer of the electron to Cu_A and then heme *a* and uptake of the pump proton. These states are common to both models. (B) Transfer of the electron from heme *a* to heme a_3 and then Cu_B with uptake of a substrate proton and ejection of the pump proton for model I. (C) Transfer of the electron from heme *a* to heme a_3, uptake of the substrate proton, ejection of the pump proton and the transfer of the electron and substrate proton to Cu_B for model II.

concentration, CytOx turnover was saturated by oxygen and the heme oxidation state was independent of oxygen concentration. As the cells became anoxic, hemes b_H, b_L, c_1 and Cyt*c* became reduced as would be expected. Addition of FCCP led to transient oxidations in heme b_H, heme c_1 and Cyt*c* which can be attributed to the small quantity of oxygen that is dissolved in the FCCP solution and that was subsequently consumed. This is borne out in the oxygen trace which shows a transient increase of ≈0.2 μM. However, FCCP caused a substantial and sustained oxidation in heme b_L consistent with the collapse in $\Delta\Psi$ causing an oxidation of heme b_L with respect to heme b_H.

Oxidation changes in heme *a* (described as a_T in the figures) were calculated from the sum of oxidation changes in a_H and a_L. Heme *a* reduced on anoxia as expected but, within the framework of the neoclassical model, heme a_3 remained partially oxidized as determined by the high occupancy of a_H. This is borne out by the heme a_3 trace, although the heme a_3 trace has a lower signal to noise and is more susceptible to drift because its spectrum is weaker and broader than the other hemes. On addition of FCCP, heme *a* remained fully reduced and heme a_3 also became reduced as indicated by the switch from a_H to a_L and a reduction in heme a_3.

3.2. Redox titrations

Oxidative redox titrations were performed in the cells without addition of exogenous redox mediators by inhibiting entry of electrons into the electron transport chain at complex I with a low concentration of rotenone in the presence of a low concentration of oxygen acting as an oxidant. The oxidation state of Cyt*c* was used as an indicator of the ambient redox potential. It was found that this procedure caused the oxidation state of Cyt*c* to vary from nearly fully reduced to nearly fully oxidized over a period of several minutes and, as data collection occurred every half second, this allowed several hundred data points to be collected as the redox potential of Cyt*c* was swept from low to high values.

Fig. 4A shows representative traces of oxidation changes in Cyt*c*, heme *a*, a_H and a_L from the chamber operating in oximetry mode when ΔP was collapsed using a combination of oligomycin and FCCP. Initially, oxygen concentration was saturating and was decreased to anoxia at time zero resulting in the reduction of Cyt*c* and heme *a* but heme *a* remained in the a_H form. Oligomycin inhibits the ATP synthase and resulted in a slow conversion of a_H to a_L. Addition of FCCP accelerated this conversion suggesting that heme *a* was maintained in the a_H form by the presence of $\Delta\Psi$ resulting from glycolytic ATP reversing the synthase.

The cells were treated with 50 nM of rotenone at 5 min and then the oxygen fraction in the tubing was increased from 0.00 to 0.05 at 6 min causing the oxygen concentration in the chamber to rise until the oxygen consumption by the cells matched the oxygen delivery. It was estimated that a tubing oxygen fraction of 0.05 would lead to a cellular oxygen consumption that was ≈20% of the oxygen consumption at saturating (baseline) oxygen tension. Baseline mitochondrial oxygen consumption was 28.9 ± 4.1 μM/min, CytOx content was 30.2 ± 3.8 nM so that baseline CytOx turnover was ≈16O_2/s and the turnover during the titration would have been less than 3.2O_2/s. The initiation of low rates of turnover resulted in a partial switch in

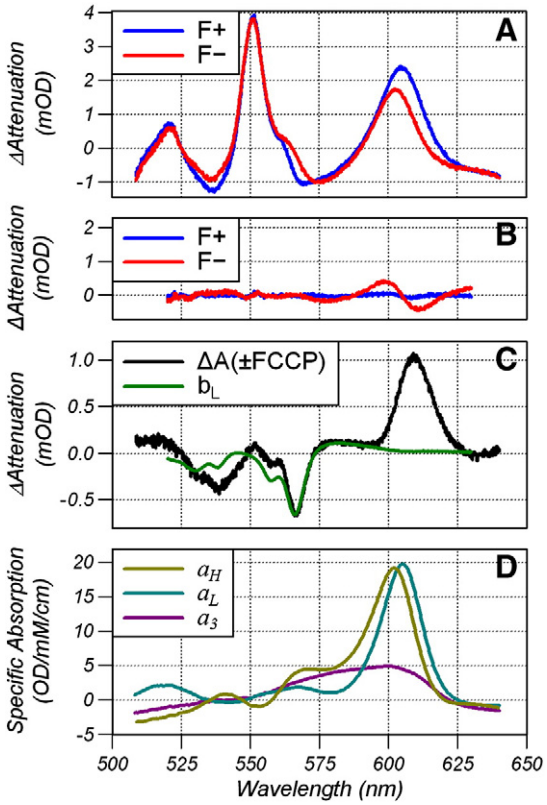

Fig. 2. (A) Oxygenated-anoxic difference attenuation spectra with (F+) and without (F−), 1 μM FCCP. (B) Residuals (data-model) of the fitting model when the spectra in A are fitted with components b_H, b_L, c_1, Cyt a_L and a_3. (C) Difference attenuation spectrum on addition of FCCP with the component of b_L that is fitted into the spectrum. (D) Reconstructed specific absorption spectra of a_H compared to the literature spectra of heme *a* (assumed to be a_L) and a_3 taken from [27].

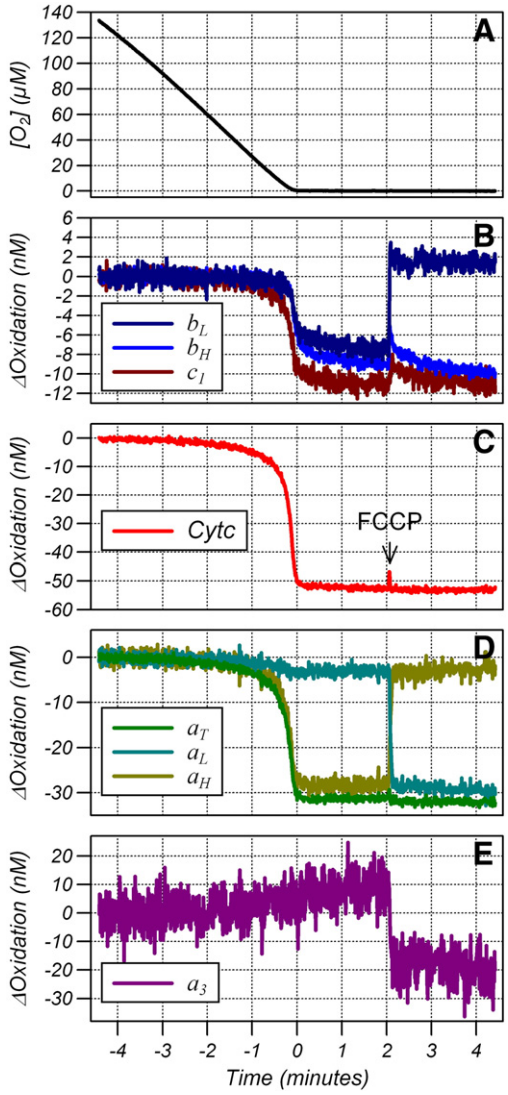

Fig. 3. Traces of oxygen concentration (A) and oxidation changes of b_H, b_L, c_1 (B), Cyt*c* (C) and CytOx (D), as the cells consume oxygen to anoxia and subsequent addition of 1 μM of FCCP (arrow). A downward deflection denotes reduction or increased occupancy.

heme *a* from the a_L to a_H form consistent with a small rise in $\Delta\Psi$ due to the onset of low rates of proton pumping.

The combination of rotenone and oxygen caused the electron transport chain to slowly oxidize and swept the redox potential of Cyt*c* from low to high values. Finally, the cells were treated with a high concentration of rotenone (1 μM) and reoxygenated by increasing the oxygen fraction in the tubing to 0.95 to fully oxidize the electron transport chain.

Fig. 4B shows representative traces of oxidation changes in CytOx and Cyt*c* as a redox titration was performed when ΔP was maintained by glycolytic ATP. Initially, oxygen concentration was saturating and was decreased to anoxia at time zero by switching the oxygen in the tubing to zero. Anoxia resulted in the reduction of Cyt*c* and heme *a* but heme *a* remained predominantly in the a_H form. Cells were treated with 50 nM rotenone at 2 min and the oxygen in the tubing was increased to 0.05 at 3 min oxidizing the electron transport chain. A second dose of 50 nM was given at 7 min to further oxidize the electron transport chain and then the cells were treated with 1 μM rotenone and reoxygenated to fully oxidize the electron transport chain.

The redox titrations, with and without FCCP, were performed in paired experiments on cells from the same culture and the paired experiments were performed six times on cells from independent cultures. The oxidation state of Cyt*c* and heme *a*, and the fractional occupation of a_H and a_L, were calculated assuming Cyt*c* and heme *a* were fully reduced during anoxia and fully oxidized at high oxygen concentration after the high dose of rotenone. The redox potential of Cyt*c* was calculated using a Nernst relationship using a midpoint potential of 260 mV [18]. The data analysis was limited to the range of 180–340 mV, equivalent to an oxidation state of 5%–95% oxidized, because outside this range small errors in Cyt*c* oxidation state result in large errors in Cyt*c* redox potential.

The redox titrations with FCCP were fitted with a 4-state redox cooperativity model following Hendler and Westeroff [21] and the data from Fig. 4A is shown with the fit in Fig. 5A. The redox titrations without FCCP could not be fitted with a neoclassical model because the lower transition, if present, was not sampled by the data. Instead, heme *a* was fitted as an $n=1$ Nernst function and the data from Fig. 4B is shown with the fit in Fig. 5B. Fig. 5C shows the relationship between reduction of heme *a* and occupancy of a_L and a_H to Cyt*c* redox potential during the onset of anoxia from a representative experiment along with a fit with an $n=1$ Nernst function. The reduction state of heme *a* fitted a Nernst function at the later stages of the anoxia (low Cyt*c* redox potential) but was more oxidized than predicted at early stages of the anoxia suggesting that the E_m of heme *a* rose during the onset of anoxia when $\Delta\Psi$ would be expected to be decreasing. The fitting parameters and the shift in the E_m of a_H from the redox titration with FCCP are shown in Table 1.

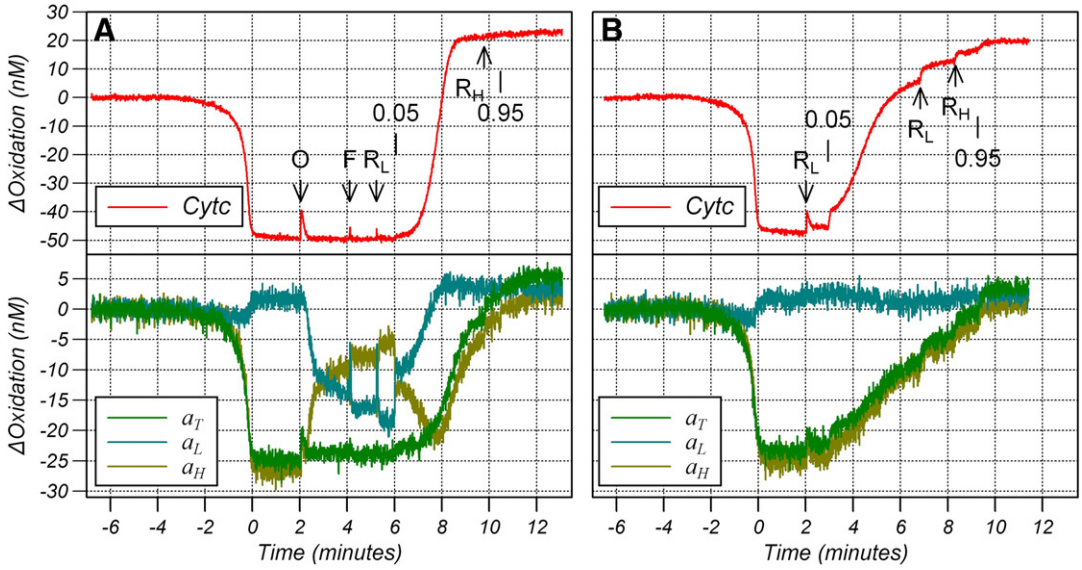

Fig. 4. Oxidation changes in heme *a* and Cyt*c* during a redox titration in the presence (A) and absence (B) of oligomycin and FCCP. The cells were initially at a saturating oxygen concentration and made anoxic at time zero. Additions to the chamber are marked with arrows and were O: oligomycin, *F*: 200 nM FCCP, R_L: 50 nM rotenone, R_H: 1 μM rotenone. Changes in the oxygen fraction in the silicone tubing are marked with lines. A downward deflection denotes reduction or increased occupancy.

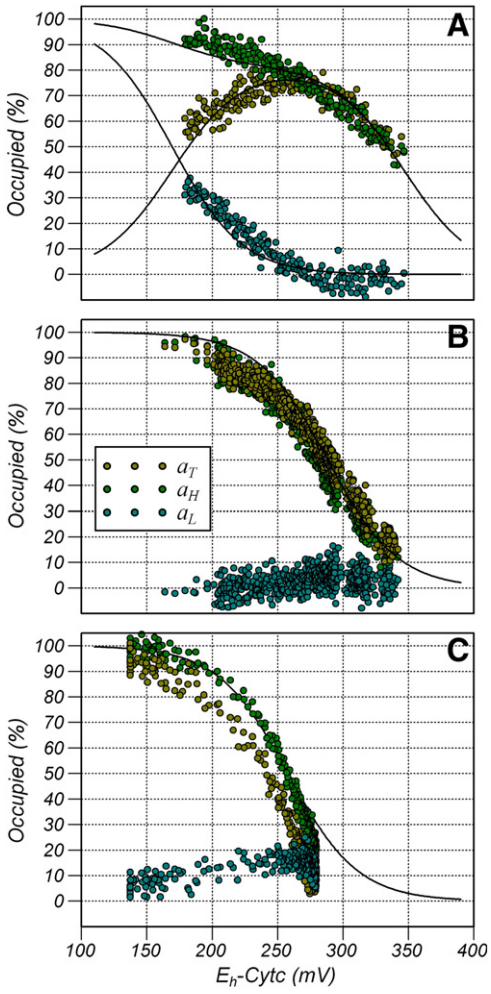

Fig. 5. Reduction of heme *a* (a_T) and occupancy of a_H and a_L plotted against Cyt*c* redox potential. (A) During a redox titration in the presence of FCCP. (B) During a redox titration in the absence of FCCP. (C) During the onset of anoxia. For A, the lines are a fit to the 4-parameter neoclassical model and B and C are a fit with an $n=1$ Nernst function to heme *a*.

3.3. Stochastic models

Both model I and model II reproduced the time course of oxidation changes in heme *a* and Cu_A from a kinetic study (see Fig. 6A and C, respectively) but the third phase was slower in model II and heme *a* showed slightly greater reduction in the second phase because the electron is not transferred to heme a_3. Model I pumped 0.90 protons whereas model II pumped 0.70 protons.

Redox titrations for model I and II are shown in Fig. 6B and D, respectively. Cu_A titrates as an $n=1$ Nernst function with an E_m of 250 mV in both models (data not shown) as would be expected and validates the algorithm for simulating a redox titration. The Cu_B center also titrated as a simple $n=1$ Nernst function in both models but with an effective E_m of 580 mV rather than the 460 mV with which it acts when it accepts an electron from heme a_3 (see Fig. 1B). The increase in the effective E_m was caused by the pumped proton which was left in an excited state after the electron left heme *a* but was not released until after Cu_B was reduced. The result was that the lowest energy state with Cu_B reduced was 120 mV below the energy level of the state that accepted the electron from heme a_3.

Heme *a* and heme a_3 titrated with an E_m of 360 mV for the first electron and with an E_m of 480 mV for the second electron using the parameters of model I. This redox cooperativity is contrary to the observed redox anti-cooperativity. The effective E_m was given by the sum of the E_m without a proton binding, the energy required to bind a proton and the interaction energy. This amounts to -270 mV $+120$ mV -210 mV $=-360$ mV for heme *a* and -130 mV $+120$ mV -350 mV $=-360$ mV for heme a_3 for the first electron. The proton was already bound for the second electron so that it did not incur an energy penalty. The effective midpoints were then -270 mV -210 mV $=-480$ mV and -130 mV -350 mV $=-480$ mV for heme *a* and heme a_3, respectively. Finally, this model predicts that the pump proton will be bound whenever heme *a* is reduced and so cannot reproduce the spectral changes observed in the redox titrations.

In contrast, model II predicts redox anti-cooperativity between heme *a* and heme a_3. The pump site was protonated when heme *a* was reduced and the substrate site was protonated when heme a_3 was reduced. Ejection of the pump site proton was aided by the electrostatic effect of the substrate proton but was not necessary to

Table 1
Midpoint potentials in millivolts calculated by fitting the modified neoclassical model to the data from redox titrations with FCCP and by fitting a Nernst function to heme *a* from redox titrations without FCCP and from the onset of anoxia.

Experiment	$E_m^{a_H}$	$E_m^{a_L}$	$E_m^{a_{3H}}$	$E_m^{a_{3L}}$	$E_m^{a_H}$	$\Delta E_m^{a_H}$	$E_m^{a_H}$	$\Delta E_m^{a_H}$
	With FCCP				Without FCCP		Anoxia	
1	338.3	215.8	309.4	186.9	289.4	48.9	261.0	77.3
2	341.9	202.9	309.2	170.2	290.4	51.5	261.5	80.4
3	337.8	213.9	303.9	180.1	287.4	50.4	266.9	70.9
4	333.5	229.3	309.1	204.8	284.6	48.9	259.9	73.7
5	341.2	214.6	301.4	174.8	288.2	52.9	258.4	82.7
6	332.6	232.3	309.3	209.1	292.7	39.9	257.8	74.8
Mean ± SD	337.6 ± 3.5	218.2 ± 9.9	307.1 ± 3.2	187.7 ± 14.6	288.8 ± 2.5	48.8 ± 4.2	260.9 ± 3.0	76.6 ± 4.1

$\Delta E_m^{a_H}$ is the shift in midpoint potential of a_H from redox titration with FCCP. $E_m^{a_H}$and $E_m^{a_L}$ are the midpoint potentials of a_H, a_L. $E_m^{a_{3H}}$ and $E_m^{a_{3L}}$ are the midpoint potentials of heme a_3 when it has a high and low potential, respectively, and $\Delta E_m^{a_H}$is the change in midpoint potential from the redox titration with FCCP.

explain the high E_m of heme *a* and heme a_3 for single electron reduction. However, the strong anti-cooperativity between the two proton sites forbids uptake of a second proton when the second electron arrives so that heme *a* and heme a_3 act with an effective E_m of 270 and 130 mV, respectively. As heme *a* has the higher E_m, only the state in which both hemes are reduced and the proton resides on the heme a_3 binding center was sampled during the redox titration. The end result was that heme *a* and a_3 appear to titrate with an effective E_m of 360 and 270 mV for the first and second electron, respectively, when this 16-state system (2 redox centers and 2 proton sites) is analyzed with a simple 4-state redox cooperativity model. Finally, the fractional occupation of a_H and a_L correspond precisely to the occupancy of heme *a* when it acts with a high or low E_m, respectively. Overall, the results of model II showed good qualitative agreement to the data reproducing both redox anti-cooperativity and the observed spectral changes.

4. Discussion

Spectral changes have been observed in the α-band of CytOx during redox titrations [13,14,30], after CO photolysis in the mixed valence enzyme [31], after photo injection of an electron in the Cu_A site [24] and stopped-flow mixing with reduced Cyt*c* [32] but there have been few attempts to assign these spectral changes to specific states of the enzyme. The Wilson et al. interpretation [13,14], but see also [30], assigns the 602 and 608 nm spectral features to heme *a* and heme a_3, respectively. If these spectral components are used for spectral fitting then the 602 and 608 nm components follow a_T and a_L, respectively, due to the linear nature of the fitting algorithm. However, this interpretation has been rejected [15] on the grounds that redox titrations in which heme a_3 is held reduced by the presence of carbon monoxide, show a single spectral feature with near equal magnitude to the fully reduced-oxidized difference spectrum [12].

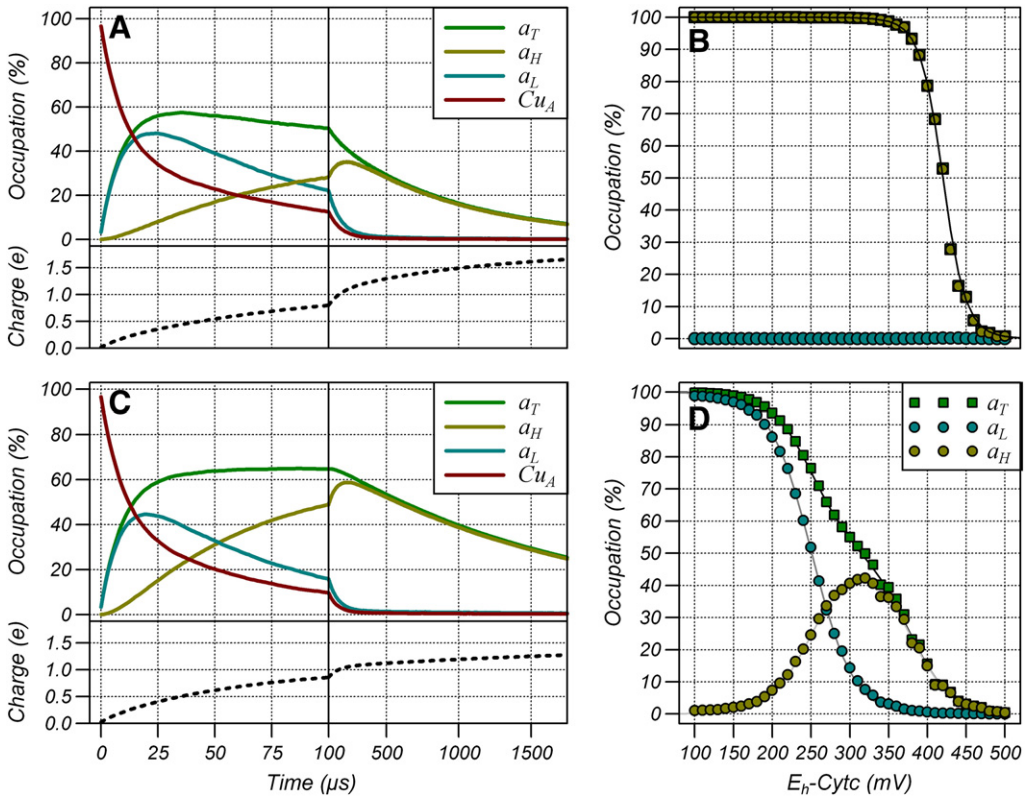

Fig. 6. Results of the stochastic simulations for model I (A and B) and model II (C and D). A and C temporal evolution of the reduction state of Cu_A and heme *a*, and charge transfer system when Cu_A is reduced, the other redox centers are oxidized and the proton sites are empty at $t = 0$. B and D simulated redox titrations. The data points are from the simulation and the lines are from a fit using a 4-state redox cooperativity model.

Furthermore, magnetic circular dichroism redox titrations of both heme *a* and heme a_3 show they titrate together [18]. More sophisticated analysis has been performed with single value decomposition algorithms [33,34] but a fundamental assumption of that analysis was that the spectral components titrate with a Nernst functional form whereas a_H clearly does not titrate in that way. It has been previously proposed that the absorption peak of the oxidized minus half-reduced enzyme is 603–604 nm whereas the peak of the oxidized minus fully reduced enzyme is at 605 nm [15,35], consistent with the spectra and interpretation presented here. However, this is the first time that the spectral features of CytOx in the α-band region have been separated, quantified and interpreted in terms of the effective E_m of heme *a* resulting from protonation events.

Within the framework of the neoclassical model, the observation that a_L and a_H titrate as the low and high potential components of heme *a* would suggest that the spectrum of heme *a* depends on the oxidation state of heme a_3. This is unlikely to be the case because the difference spectrum of heme *a* has a peak at 605 nm when either a_3 is held reduced with carbon monoxide [15] or held oxidized with cyanide [27,36]. In addition, time resolved studies show that heme *a* has an absorption peak at 605 nm when an electron is initially injected into the oxidized enzyme [24,32], a time when the neoclassical model would predict that heme *a* has a high potential and hence an absorption at 602 nm.

In the absence of proton binding, the effective E_m of heme *a* with respect to cytochrome *c* should decrease with increasing $\Delta\Psi$ by a factor equal to the dielectric depth of heme *a* because the electron has to move against the electric field. Quantification of the mitochondrial membrane potential from living cells is error prone but previous studies have estimated a baseline value of 150 mV [37]. This would seem to be compatible with a shift of 48.6 mV in the E_m of a_H between redox titrations in the presence and absence of oligomycin and FCCP assuming a dielectric depth of 0.34. However, $\Delta\Psi$ was unlikely to be zero in the presence of oligomycin at this relatively low concentration of FCCP when the electron transport chain was still pumping protons at 20% of normal values. Furthermore, $\Delta\Psi$ should be considerably lower than 150 mV when it is maintained by glycolytic ATP reversing the ATP synthase rather than under normal turnover conditions when $\Delta\Psi$ drives the ATP synthase forward. Finally, the shift in the E_m of a_H of greater than 76 mV on the onset of anoxia when $\Delta\Psi$ is expected to be close to 150 mV is incompatible with a dielectric depth of 0.34. Therefore, formation of a_H must involve a greater movement of charge against $\Delta\Psi$ than can be accounted for by the electron moving from Cyt*c* to heme *a*. The most obvious candidate for this movement of charge is the uptake of a proton. The binding of the proton at the pump site could be directly responsible for the change in E_m and spectrum of heme *a*. Alternatively, proton binding could trigger a conformational change that alters the spectrum of heme *a* or a conformational change could alter the E_m and spectrum of heme *a* and the pKa of the pump site. Conformational changes of the arginines above the propionates of heme *a* (R481 and R482, R. sphaeroides numbering) have been proposed [38] and point mutations of R481 generate shifts in the spectra of heme *a* of similar magnitude seen here [39].

The goal of the stochastic simulations is to use the kinetic parameters of the first electron reduction of CytOx (O to E transition) to predict the reduction by the second, third and fourth electron as occurs in a redox titration. It is already known that the kinetic parameters of the additional electrons must be different from the first electron and this approach is able to identify those differences. An obvious failure of model I is that it does not include a substrate proton on the second electron reduction of the binuclear center (E to R transition) and there is no obvious way to include protonation interactions as heme a_3 would already have a high midpoint potential due to the interaction with the pump proton. The model accurately predicts the uptake of three protons on the 4 electron reduction of the oxidized enzyme but it predicts two pump protons and one substrate proton rather than one pump proton and two substrate protons. Finally, heme *a* and a_3 titrate with redox cooperativity rather than the anti-cooperativity as is observed.

Model II attempts to implement the proton pumping scheme of West et al. [40] in which the pumped proton is taken up faster than the substrate proton to neutralize the negative charge of the electron at heme *a*. The subsequent uptake of the substrate proton, which binds more tightly to the electron at heme a_3, then ejects the pump proton through electrostatic repulsion. In this model, the midpoint potential of heme *a* is dependent on the pump proton, having an E_m of 270 and 360 mV in the absence and presence of the proton, whereas the E_m of heme a_3 is dependent on the substrate proton, having an E_m of 130 and 360 mV in the absence and presence of the proton (see Fig. 1C). Redox anti-cooperativity occurs because the pump and the substrate proton binding sites cannot be occupied simultaneously due to the electrostatic repulsion. The lower E_m for the second electron observed in redox titrations (218 mV) compared to the simulations (270 mV) could be the result of a residual electrostatic interaction between the electrons on heme *a* and a_3 but it should be much smaller than would be predicted from a simple electrostatic calculation considering the separation of the hemes because it would be counteracted by the charge on the substrate proton. Model II predicts that the pump proton binding site is empty in the fully reduced enzyme and so explains why the 602 nm spectrum is only observed at intermediate levels of reduction. It also means that any conformational change that accompanies the uptake of the pump proton and alteration in the E_m of heme *a* would not be observed in the crystal structure of the fully oxidized or fully reduced enzyme. Likewise, heme *a* titrates with a peak at 605 nm in the CO-bound and CN-bound enzyme indicating that the pump site is empty and any conformational change would not be apparent in the CO-bound crystal structure.

This model could also account for the failure to reduce heme a_3 under anoxic conditions when ΔP is maintained by glycolytic ATP. Reduction of heme a_3 requires uptake of the substrate proton and ejection of the pump proton against ΔP and, for a given ΔP, this will decrease the effective E_m of heme a_3 substantially more than it decreases the effective E_m of heme *a*. Furthermore, the residual $\Delta\Psi$ during the titration with FCCP could account for the apparent difference in midpoint potentials of the two hemes. Taking these effects into account, the data from the redox titration in the presence of FCCP are in good agreement with those of the isolated enzyme. These effects could be confirmed by performing titrations at intermediate values of ΔP. Furthermore, quantifying the shift in midpoint potentials of heme *a* and heme a_3 with $\Delta\Psi$ should provide further information with regard to the location of the pump proton site and pumping mechanism.

5. Conclusion

The data and stochastic simulations presented here are consistent with a model in which uptake of the pumped proton alters the midpoint potential of heme *a*, blueshifts its α-band absorption peak from 605 to 602 nm and, in combination with the substrate proton altering the E_m of heme a_3, gives rise to much of the apparent redox anti-cooperativity observed in redox titrations. Multi-wavelength decomposition of α-band attenuation spectra into the a_H and a_L components should be invaluable in interpreting a variety of optical studies as it should provide additional information to track the proton uptake and protonation status of the pump site.

Acknowledgments

The authors wish to thank Torsten Merbitz-Zahradnik and Bernard Trumpower for their help in measuring the bc_1 specific absorption

spectra. This work was supported by grant numbers R01NS054298 and 5R21RR25803 from the National Institutes of Health.

References

[1] I. Belevich, M.I. Verkhovsky, Molecular mechanism of proton translocation by cytochrome *c* oxidase, Antioxid. Redox Signal. 10 (1) (2008) 1–29.
[2] S. Iwata, C. Ostermeier, B. Ludwig, H. Michel, Structure at 2.8 A resolution of cytochrome c oxidase from Paracoccus denitrificans, Nature 376 (6542) (1995) 660–669.
[3] T. Tsukihara, H. Aoyama, E. Yamashita, T. Tomizaki, H. Yamaguchi, K. Shinzawa-Itoh, R. Nakashima, R. Yaono, S. Yoshikawa, The whole structure of the 13-subunit oxidized cytochrome c oxidase at 2.8 A, Science 272 (5265) (1996) 1136–1144.
[4] M. Wikstrom, M.I. Verkhovsky, Mechanism and energetics of proton translocation by the respiratory heme–copper oxidases, Biochim. Biophys. Acta 1767 (10) (2007) 1200–1214.
[5] K. Faxen, G. Gilderson, P. Adelroth, P. Brzezinski, A mechanistic principle for proton pumping by cytochrome c oxidase, Nature 437 (7056) (2005) 286–289.
[6] M. Wikstrom, M.I. Verkhovsky, G. Hummer, Water-gated mechanism of proton translocation by cytochrome c oxidase, Biochim. Biophys. Acta 1604 (2) (2003) 61–65.
[7] K. Shimokata, Y. Katayama, H. Murayama, M. Suematsu, T. Tsukihara, K. Muramoto, H. Aoyama, S. Yoshikawa, H. Shimada, The proton pumping pathway of bovine heart cytochrome c oxidase, Proc. Natl Acad. Sci. U.S.A. 104 (10) (2007) 4200–4205.
[8] P. Nicholls, C.E. Cooper, J.M. Wrigglesworth, Control of proteoliposomal cytochrome c oxidase: the overall reaction, Biochem. Cell Biol. 68 (9) (1990) 1128–1134.
[9] P. Nicholls, Control of proteoliposomal cytochrome c oxidase: the partial reactions, Biochem. Cell Biol. 68 (9) (1990) 1135–1141.
[10] D.F. Wilson, W.L. Rumsey, T.J. Green, J.M. Vanderkooi, The oxygen dependence of mitochondrial oxidative phosphorylation measured by a new optical method for measuring oxygen concentration, J. Biol. Chem. 263 (6) (1988) 2712–2718.
[11] R. Acin-Perez, E. Salazar, M. Kamenetsky, J. Buck, L.R. Levin, G. Manfredi, Cyclic AMP produced inside mitochondria regulates oxidative phosphorylation, Cell Metab. 9 (3) (2009) 265–276.
[12] A. Tzagoloff, D.C. Wharton, Studies on the electron transfer system. Lxii. The reaction of cytochrome oxidase with carbon monoxide, J. Biol. Chem. 240 (1965) 2628–2633.
[13] D.F. Wilson, J.G. Lindsay, E.S. Brocklehurst, Heme–heme interaction in cytochrome oxidase, Biochim. Biophys. Acta 256 (2) (1972) 277–286.
[14] J.G. Lindsay, D.F. Wilson, Apparent adenosine triphosphate induced ligand change in cytochrome a3 of pigeon heart mitochondria, Biochemistry 11 (24) (1972) 4613–4621.
[15] M.K.F. Wikstrom, H.J. Harmon, W.J. Ingledew, B. Chance, A re-evaluation of the spectral, potentiometric and energy-linked properties of cytochrome c oxidase in mitochondria, FEBS Lett. 65 (3) (1976) 259–277.
[16] P. Nicholls, L.C. Petersen, Haem–haem interactions in cytochrome aa3 during the anaerobic–aerobic transition, Biochim. Biophys. Acta 357 (3) (1974) 462–467.
[17] P.A. Harmon, R.W. Hendler, I.W. Levin, Resonance Raman and optical spectroscopic monitoring of heme a redox states in cytochrome c oxidase during potentiometric titrations, Biochemistry 33 (3) (1994) 699–707.
[18] N. Kojima, G. Palmer, Further characterization of the potentiometric behavior of cytochrome oxidase. Cytochrome alpha stays low spin during oxidation and reduction, J. Biol. Chem. 258 (24) (1983) 14908–14913.
[19] E.A. Gorbikova, K. Vuorilehto, M. Wikstrom, M.I. Verkhovsky, Redox titration of all electron carriers of cytochrome c oxidase by Fourier transform infrared spectroscopy, Biochemistry 45 (17) (2006) 5641–5649.
[20] P. Nicholls, J.M. Wrigglesworth, Routes of cytochrome a3 reduction. The neoclassical model revisited, Ann. NY Acad. Sci. 550 (1988) 59–67.
[21] R.W. Hendler, H.V. Westerhoff, Redox interactions in cytochrome c oxidase: from the "neoclassical" toward "modern" models, Biophys. J. 63 (6) (1992) 1586–1604.
[22] D.F. Blair, W.R. Ellis Jr., H. Wang, H.B. Gray, S.I. Chan, Spectroelectrochemical study of cytochrome c oxidase: pH and temperature dependences of the cytochrome potentials. Characterization of site–site interactions, J. Biol. Chem. 261 (25) (1986) 11524–11537.
[23] L.I. Krishtalik, The negative cooperativity in cytochrome c oxidase redox reactions: the electrostatic effect, Arch. Biochem. Biophys. 243 (2) (1985) 701–702.
[24] I. Belevich, D.A. Bloch, N. Belevich, M. Wikstrom, M.I. Verkhovsky, Exploring the proton pump mechanism of cytochrome c oxidase in real time, Proc. Natl Acad. Sci. U.S.A. 104 (8) (2007) 2685–2690.
[25] V.S. Hollis, M. Palacios-Callender, R.J. Springett, D.T. Delpy, S. Moncada, Monitoring cytochrome redox changes in the mitochondria of intact cells using multi-wavelength visible light spectroscopy, Biochim. Biophys. Acta 1607 (2–3) (2003) 191–202.
[26] S.J. Matcher, M. Cope, D.T. Delpy, Use of the water absorption spectrum to quantify tissue chromophore concentration changes in near-infrared spectroscopy, Phys. Med. Biol. 39 (1) (1994) 177–196.
[27] G.L. Liao, G. Palmer, The reduced minus oxidized difference spectra of cytochromes a and a3, Biochim. Biophys. Acta 1274 (3) (1996) 109–111.
[28] D.T. Gillespie, Exact stochastic simulation of coupled chemical reactions, J. Phys. Chem. 81 (25) (1977) 2340–2361.
[29] S. Ransac, N. Parisey, J.P. Mazat, The loneliness of the electrons in the bc1 complex, Biochim. Biophys. Acta 1777 (7–8) (2008) 1053–1059.
[30] P. Hellwig, S. Grzybek, J. Behr, B. Ludwig, H. Michel, W. Mantele, Electrochemical and ultraviolet/visible/infrared spectroscopic analysis of heme a and a3 redox reactions in the cytochrome c oxidase from Paracoccus denitrificans: separation of heme a and a3 contributions and assignment of vibrational modes, Biochemistry 38 (6) (1999) 1685–1694.
[31] M.I. Verkhovsky, A. Jasaitis, M. Wikstrom, Ultrafast haem–haem electron transfer in cytochrome c oxidase, Biochim. Biophys. Acta 1506 (3) (2001) 143–146.
[32] L.E. Andreasson, Characterization of the reaction between ferrocytochrome c and cytochrome c oxidase, Eur. J. Biochem. 53 (2) (1975) 591–597.
[33] R.W. Hendler, K.V. Reddy, R.I. Shrager, W.S. Caughey, Analysis of the spectra and redox properties of pure cytochromes aa3, Biophys. J. 49 (3) (1986) 717–729.
[34] K.V. Reddy, R.W. Hendler, B. Bunow, Complete analysis of the cytochrome components of beef heart mitochondria in terms of spectra and redox properties. Cytochromes aa3, Biophys. J. 49 (3) (1986) 705–715.
[35] R.H. Tiesjema, A.O. Muijsers, B.F. van Gelder, Biochemical and biophysical studies on cytochrome c oxidase. X. Spectral and potentiometric properties of the hemes and coppers, Biochim. Biophys. Acta 305 (1) (1973) 19–28.
[36] A.J. Moody, P.R. Rich, The effect of pH on redox titrations of haem a in cyanide-liganded cytochrome-c oxidase: experimental and modelling studies, Biochim. Biophys. Acta 1015 (2) (1990) 205–215.
[37] D.G. Nicholls, M.W. Ward, Mitochondrial membrane potential and neuronal glutamate excitotoxicity: mortality and millivolts, Trends Neurosci. 23 (4) (2000) 166–174.
[38] P. Brzezinski, G. Larsson, Redox-driven proton pumping by heme–copper oxidases, Biochim. Biophys. Acta 1605 (1–3) (2003) 1–13.
[39] H.J. Lee, L. Ojemyr, A. Vakkasoglu, P. Brzezinski, R.B. Gennis, Properties of Arg481 mutants of the aa3-type cytochrome c oxidase from Rhodobacter sphaeroides suggest that neither R481 nor the nearby D-propionate of heme a3 is likely to be the proton loading site of the proton pump, Biochemistry 48 (30) (2009) 7123–7131.
[40] P.R. Rich, B. Meunier, R. Mitchell, A. Moody, P. Mitchell, Coupling of charge and proton movement in cytochrome c oxidase, Biochim. Biophys. Acta 1275 (1986) 91–95.